Rare Metal Materials and Engineering
Volume 55, Issue 10, October 2026
Available online at www.rmme.ac.cn

Science Press

Cite this article as: Liu Wenli, Zhao Xia, Hou Kunlei, et al. Effect of Carbon Content on Microstructure and Mechanical Properties of a Novel Wrought Nickel-Based Superalloy[J]. Rare Metal Materials and Engineering, 2026, 55(10): 2463-2475. DOI: https://doi.org/10.12442/j.issn.1002-185X.20250507.

ARTICLE

Effect of Carbon Content on Microstructure and Mechanical Properties of a Novel Wrought Nickel-Based Superalloy

Liu Wenli[1,2,3], Zhao Xia[2,3], Hou Kunlei[2,3], Wang Yifei[4], Wang Ping[1], Ma Yingche[2,3], Hao Xianchao[2,3], Ou Meiqiong[2,3]

[1] School of Materials Science and Engineering, Northeastern University, Shenyang 110819, China; [2] Shi-changxu Innovation Center for Advanced Materials, Institute of Metal Research, Chinese Academy of Sciences, Shenyang 110016, China; [3] Key Laboratory of Nuclear Materials and Safety Assessment, Institute of Metal Research, Chinese Academy of Sciences, Shenyang 110016, China; [4] Sinotest Equipment Co., Ltd, Changchun 130103, China

Abstract: Carbon (C), as a crucial trace element in nickel-based superalloys, exerts a significant influence on mechanical properties even with minor variations in content. This study investigated the effect of C content on the microstructure and mechanical properties of a novel nickel-based superalloy GH4750. The results demonstrate that with increasing C content from 0.024wt% to 0.042wt% and then to 0.082wt%, the quantity and average size of M_C carbides increase. These carbides can effectively pin grain boundaries, resulting in a progressive reduction in grain size from approximately 35 μm to approximately 31 μm and ultimately to approximately 22 μm. Both the room-temperature and 750 °C tensile strengths initially increase and then decrease as the C content increases. Conversely, the elongation displays the opposite trend. The differences in tensile properties are closely related to the carbide characteristics. An appropriate increase in carbide content can inhibit the formation and coalescence of microvoids, effectively pin grain boundaries, and prevent grain boundary slip at elevated temperatures. Excessive carbides act as preferential sites for microcrack initiation. The stress-rupture life decreases with increasing C content, attributed to the larger grain size. Based on comprehensive consideration, the optimal C content for the novel nickel-based superalloy GH4750 is determined to be 0.042wt%.

Key words: nickel-based superalloys; carbon content; mechanical properties; fracture mechanism

1 Introduction

Nickel-based superalloys, owing to their outstanding high-temperature properties, are extensively employed in the hot-section components of aero-engines, accounting for 40%–60% of engine mass[1]. To achieve higher thrust-to-weight ratios, advanced aero-engines require improved temperature capability in structural materials[2], driving the gradual replacement of conventional alloy steels by superalloys[3] and promoting the continuous upgrading of existing alloys. Among them, IN718 is the most widely used γ''-Ni_3Nb strengthened alloy, representing more than 45% of total superalloy production[4]. It exhibits excellent strength from room temperature up to 650 °C and has been broadly applied in turbine disks, cases, and other hot-section components (e.g., accounting for 57% in the PW4000 engine). However, the $\gamma'' \rightarrow \delta$ phase transformation limits the long-term service temperature of IN718 to below 650 °C, creating a bottleneck to further improvements in engine performance. For applications above 650 °C, γ'-strengthened alloys such as Waspaloy and Inconel 939 are often adopted. Nevertheless, these alloys typically contain 12wt%–20wt% Co[5–6], leading to high manufacturing costs, while their high γ' fraction makes them prone to welding cracks. K4750 is a novel Co-free cast nickel-based superalloy. It contains about 4.2wt% Al and Ti to form the strengthening phase γ'-Ni_3(Al, Ti), about 4.3wt% Mo

Received date: October 29, 2025
Corresponding author: Hou Kunlei, Ph. D., Assistant Research Fellow, Shi-changxu Innovation Center for Advanced Materials, Institute of Metal Research, Chinese Academy of Sciences, Shenyang 110016, P. R. China, E-mail: klhou17s@imr.ac.cn; Wang Ping, Ph. D., Professor, School of Materials Science and Engineering, Northeastern University, Shenyang 110819, P. R. China, E-mail: wping@epm.neu.edu.cn

and W for solid-solution strengthening, and 0.08wt% – 0.13wt% C for grain boundary (GB) strengthening[7–10]. K4750 exhibits excellent strength and good microstructural stability at 750 °C[11] and has already been applied to load-bearing frame components, such as struts, in advanced aero-engines. In addition, it demonstrates good formability, providing cast/forged dual applicability, similar to IN718 and Waspaloy. However, the role of certain alloying elements may differ significantly between wrought and cast alloys, particularly C. Previous studies[12–16] have shown that the C content in wrought superalloys (<0.08wt%) is generally much lower than that in cast alloys (0.08wt%–0.13wt% for K4750). Therefore, it is necessary to investigate the influence of C on the microstructure and mechanical properties of the new wrought alloy GH4750 to determine its optimal addition level and provide guidance for alloy design.

During processes such as casting and hot deformation (forging, rolling), C significantly influences the microstructure of alloys. First, the solubility of C in the Ni matrix is limited[17] (<0.4wt%), and during casting and solidification, it tends to segregate between dendrites (with a segregation coefficient <1). It combines with other positively segregating elements (Ti, Nb, Mo, etc) to form primary carbides, such as *M*C and M_6C[18–19]. As the C content increases, the degree of segregation also increases, thereby altering the types, quantities, and distribution of carbides. Second, during hot deformation, carbide interfaces can accumulate dislocations and other defects, which influence the dynamic recrystallization process. For instance, carbides may serve as nucleation sites to promote intragranular discontinuous recrystallization[20]. Carbides can also effectively pin GBs, thereby hindering their migration and affecting grain growth during solution heat treatment[21]. Finally, primary carbides may undergo complex phase transformations during aging or long-term service, such as $MC \rightarrow M_{23}C_6$[22] or $MC \rightarrow M_6C$[23].

The influence of C on the mechanical properties of alloys can be divided into two aspects. On the one hand, C affects the precipitation characteristics of carbides, thereby altering the alloy's mechanical properties. Blocky and rod-like *M*C carbides distributed along GBs can effectively hinder dislocation motion during plastic deformation, thereby strengthening the GBs[24]. In contrast, $M_{23}C_6$ carbides, precipitated as fine particles along the GBs, can effectively impede the coalescence of defects such as voids and microcracks, thereby preventing their aggregation and interconnection. This delays the formation of intergranular cracks and enhances the alloy's durability[7–8]. However, large, blocky, or skeleton-like primary *M*C carbides are prone to fracture under stress, forming crack initiation sites and promoting microcrack propagation[10,25]. When $M_{23}C_6$ carbides form a continuous network along the GBs, they provide a preferential path for crack propagation, thereby reducing the overall performance of the alloy[10,26].

On the other hand, carbides influence hot deformation and recrystallization, thereby affecting the alloy's microstructure, particularly grain size; for instance, Gibbons[27] and Shingledecker[28] et al reported that at low C contents (0.03wt%), larger grain sizes improve creep resistance and lead to longer fracture lifetimes. Overall, the effect of C on mechanical properties is complex, and its mechanisms need to be analyzed in conjunction with the phase composition and microstructural characteristics of specific alloy systems.

C content significantly influences processes such as solidification, hot working, and heat treatment. The carbides and secondary phases affect deformation and fracture behavior, thereby significantly influencing the mechanical properties of wrought nickel-based superalloys. In this work, the effect of C content on the microstructure of the newly developed wrought alloy GH4750 in the as-rolled and heat-treated conditions was investigated. Furthermore, room-temperature and high-temperature tensile tests, as well as creep tests, were conducted to elucidate the underlying mechanisms by which C content influences mechanical properties. Finally, the appropriate C content for the alloy was determined.

2 Experiment

The nominal chemical composition of the GH4750 alloy (wt%) was 20Cr-3W-4.5Fe-1.3Mo-1.2Al-2.8Ti-1.5Nb-*x*C, with Ni as the balance. Three alloys with different carbon levels were designed to investigate the effect of C on the microstructure and mechanical properties. The designed C contents were 0.02wt%, 0.04wt%, and 0.08wt%, which fall within the typical range for deformation superalloys. Due to unavoidable variations during vacuum melting and processing, the measured C content of the alloy sheets was 0.024wt%, 0.042wt%, and 0.082wt%. The slight excess of 0.082wt% over the designed upper limit is attributed to normal experimental variation during alloy preparation. A 25 kg ingot was prepared by vacuum induction melting and subsequently homogenized at 1200 °C for 20 h. The ingot was forged at 1180 °C into a slab measuring 1000 mm in length and 50 mm in thickness, and then hot-rolled at 1150 °C into plates measuring 1000 mm in length and 20 mm in thickness. The plates were heat-treated at 1120 °C for 4 h, then air-cooled, and subsequently held at 800 °C for 20 h, followed by air cooling. After heat treatment, cylindrical specimens (*Φ*5 mm×10 mm) were machined perpendicular to the rolling direction (RD) for room-temperature and high-temperature (750 °C) tensile tests, as well as for creep testing. For tensile testing, three parallel specimens were employed, and the average values were used to determine the ultimate tensile strength, yield strength, elongation, and reduction in area. The creep tests were conducted at 750 °C under a constant stress of 320 MPa until final fracture, from which strain-time curves were obtained.

The phase constituents of the heat-treated GH4750 alloy samples were characterized using an X-ray diffractometer (XRD, Bruker D2). The microstructures of the rolled and heat-treated alloys, including grain structures, carbides, and γ' precipitates, as well as the post-fracture longitudinal cross-sectional grain deformation and local stress/strain

distributions, were characterized using scanning electron microscope (SEM; ZEISS MERLIN and Hitachi S4800), electron backscatter diffraction (EBSD), electron probe microanalysis (EPMA; JXA-8530F), and transmission electron microscope (TEM; FEI Talos F200X). EBSD data were further processed and analyzed using AZtecCrystal software.

The XRD sample surfaces were mechanically ground to achieve a smooth, flat finish. The SEM samples were first prepared with a smooth mirror-like surface using conventional metallographic methods, followed by etching with two techniques: chemical etching with a solution of 20 g $CuSO_4$+100 mL HCl+5 mL H_2SO_4+100 mL H_2O for routine microstructural observation, and electrochemical etching with a solution of 13 mL H_3PO_4+42 mL H_2SO_4+45 mL HNO_3 for the observation of γ' precipitates, at a voltage of 1.5V and current of 0.2 A for approximately 40 s. EBSD samples were prepared by argon ion polishing to eliminate surface stress. TEM samples were prepared by cutting slices with thickness of approximately 0.5 mm, grinding them to 50 μm in thickness, punching out Φ3 mm discs, and thinning using an RL-2 twin-jet electrolytic thinning device. The electrolyte used for thinning was a mixture of 10vol% $HClO_4$ and 90vol% C_2H_5OH, with the temperature controlled at approximately − 20 ° C and an applied voltage of approximately 18 V.

3 Results and Discussion

3.1 Thermo-Calc theoretical calculations

Based on the TTNI8 nickel-based superalloy database, thermodynamic calculations were performed using Thermo-Calc for GH4750 alloys with C contents of 0.024wt% , 0.042wt%, and 0.082wt% (Fig.1). As shown in Fig.1a–1c, the equilibrium phase types and precipitation sequences are identical for the three alloys, including γ matrix, *M*C carbides, γ' phases, $M_{23}C_6$ carbides, and η phases. However, the characteristic precipitation temperatures of these phases differ significantly among the alloys (Fig.1d–1f and Table 1). With increasing C content to 0.024wt%, 0.042wt%, and 0.082wt%, the liquidus temperature ($T_{liquidus}$) decreases slightly to 1364, 1363, and 1361 °C and the solidus temperature ($T_{solidus}$) slightly increases to 1265, 1266, and 1270 ° C, respectively; consequently, the solidification range (ΔT_{L-S}) becomes narrower. For the three alloys with C contents of 0.024wt% , 0.042wt% , and 0.082wt% , the precipitation temperature of *M*C carbides (T_{MC}) increases significantly to 1270, 1290, and 1310 °C, while that of $M_{23}C_6$ carbides ($T_{M_{23}C_6}$) increases slightly to 950, 953, and 958 ° C, respectively. The γ' precipitation temperature ($T_{\gamma'}$) slightly decreases to 1000, 999, and 993 °C, respectively. Notably, the dissolution temperature of *M*C carbides exceeds the solidus, indicating that *M*C carbides nucleate and precipitate in the solid-liquid coexistence region. These carbides, often called primary carbides, are relatively large and blocky in morphology. During subsequent heat treatments, *M*C carbides cannot fully dissolve, and excessive amounts may adversely affect the mechanical properties of nickel-based superalloys[29].

3.2 DSC Analysis

Fig. 2 presents the DSC heating and cooling curves of the alloys containing 0.024wt% C, 0.042wt% C, and 0.082wt% C. As shown in Fig. 2a, three major phase transformations occur during heating. With increasing temperature, the γ' phase first

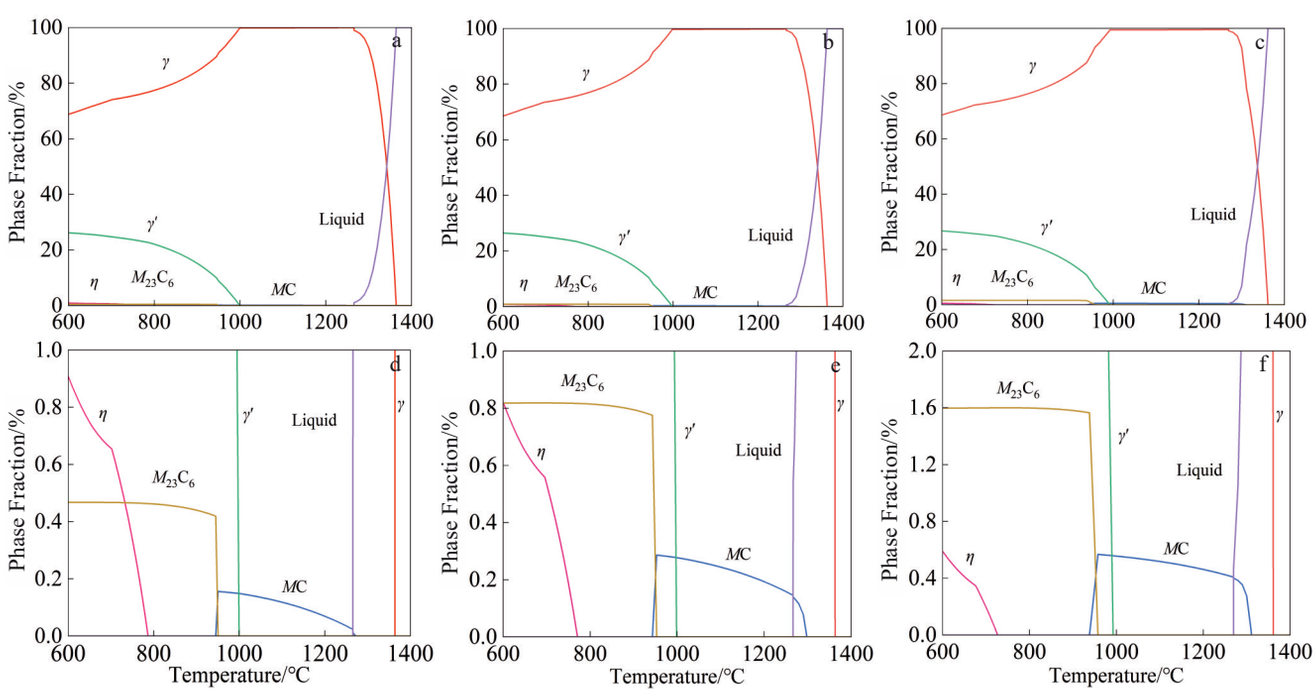

Fig.1 Equilibrium precipitates of GH4750 alloys with different C contents calculated by Thermo-Calc software at 600–1400 °C: (a, d) 0.024wt%, (b, e) 0.042wt%, and (c, f) 0.082wt%

Table 1 Phase transition temperatures of GH4750 alloy with different C contents calculated by Thermo-Calc software (℃)

C content/wt%	$T_{liquidus}$	$T_{\gamma'}$	T_{MC}	$T_{M_{23}C_6}$	$T_{solidus}$	$\Delta T_{L\text{-}S}$
0.024	1364	1000	1270	950	1265	99
0.042	1363	999	1290	953	1266	97
0.082	1361	993	1310	958	1270	91

dissolves into the γ matrix, followed by the dissolution of *M*C carbides, and finally melts into the γ matrix. The DSC cooling curves in Fig. 2b reveal that solidification also involves three sequential transformation events: (1) the γ matrix nucleates and grows rapidly from the liquid phase to form a γ dendritic network, releasing a large amount of latent heat; (2) *M*C carbides precipitate; (3) γ' precipitates form. During the late stage of solidification, the interdendritic residual liquid solidifies slowly over a wide temperature

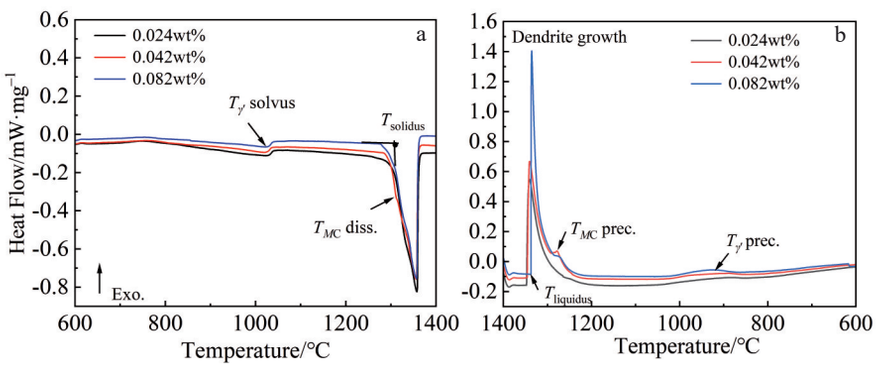

Fig.2 DSC curves of the alloys containing 0.024wt% C, 0.042wt% C, and 0.082wt% C: (a) heating process and (b) cooling process

range. For the alloys containing 0.024wt% C, 0.042wt% C, and 0.082wt% C, the solidus temperatures are 1307, 1299, and 1303 °C, while their liquidus temperatures are 1347, 1346, and 1337 °C, respectively. The transformation temperatures of *M*C carbides and γ' phase during heating and cooling, summarized in Table 2, show discrepancies between heating and cooling results for the same phase. This is attributed to the thermal hysteresis associated with phase transformations during heating and cooling. Therefore, the average value of the two is typically taken as the transformation temperature. Based on DSC analysis, the transformation temperatures of *M*C carbide for the alloys containing 0.024wt% C, 0.042wt% C, and 0.082wt% C are 1329, 1295, and 1298 °C, and the corresponding γ' phase transformation temperatures are 960, 955, and 976 ° C, respectively. The transformation temperatures predicted by Thermo-Calc in the previous section differ from the DSC experimental results. This discrepancy mainly arises because thermodynamic calculations assume equilibrium conditions, whereas real materials are not in complete equilibrium. Thus, thermodynamic equilibrium calculations can provide theoretical guidance, but experimental validation is necessary to ensure the accuracy of predictions.

3.3 Effect of C on microstructure

Fig. 3 presents the inverse pole figure (IPF) maps obtained from EBSD analysis of hot-rolled alloys containing 0.024wt% C, 0.042wt% C, and 0.082wt% C, with the IPF orientation aligned along the RD (IPF//RD). During hot rolling, static recrystallization between passes and dynamic recrystallization during deformation lead to equiaxed grains with relatively uniform size, orientation, and distribution. However, with increasing C content, the average grain size gradually

Table 2 Characteristic phase transformation temperatures of GH4750 alloys with different C contents obtained from DSC measurements (°C)

C content/wt%	Condition	$T_{liquidus}$	T_{MC}	$T_{solidus}$	$T_{\gamma'}$	$\Delta T_{L\text{-}S}$
0.024	Heating	-	1329	1307	1024	-
	Cooling	1347	-	-	896	-
	Mean value	1347	1329	1307	960	40
0.042	Heating	-	1311	1299	1020	-
	Cooling	1346	1279	-	890	-
	Mean value	1346	1295	1299	955	47
0.082	Heating	-	1324	1303	1022	-
	Cooling	1337	1271	-	930	-
	Mean value	1337	1298	1303	976	34

decreases, reaching 35.11, 31.52, and 22.05 μm for alloys containing 0.024wt% C, 0.042wt% C, and 0.082wt% C, respectively.

Fig.4 shows SEM micrographs of the hot-rolled alloys with different C contents. During deformation, carbides, due to their high modulus and poor deformability, fracture and are refined; they are subsequently randomly distributed in the deformed matrix as blocky particles that follow the metal flow. With increasing C content, the number of carbides increases significantly, with corresponding area fractions of 0.197%, 0.311%, and 0.701%. EPMA elemental mapping of the hot-rolled microstructures (Fig. 5) reveals that these dispersed blocky particles are Cr-depleted but enriched in Ti, Nb, and Mo. Point analysis at the location indicated by the arrow shows a composition of 3.46at% C, 25.80at% Ti,

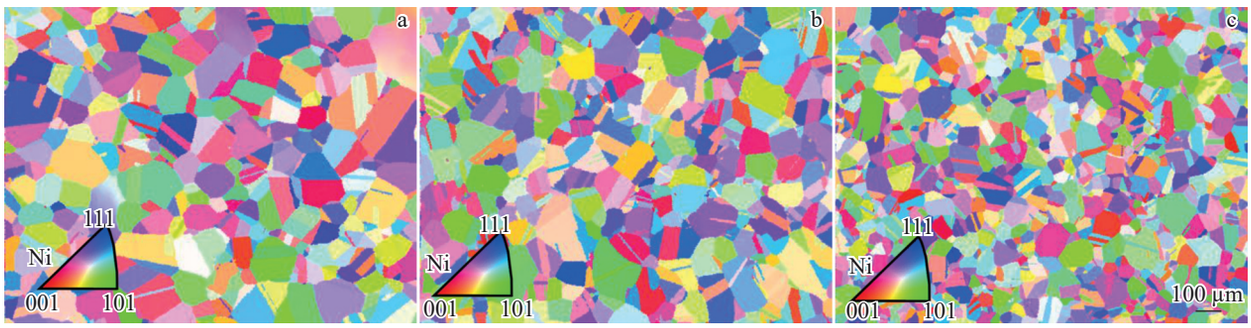

Fig.3 IPF maps showing the grain morphology of hot-rolled GH4750 alloy with different C contents: (a) 0.024wt%, (b) 0.042wt%, and (c) 0.082wt%

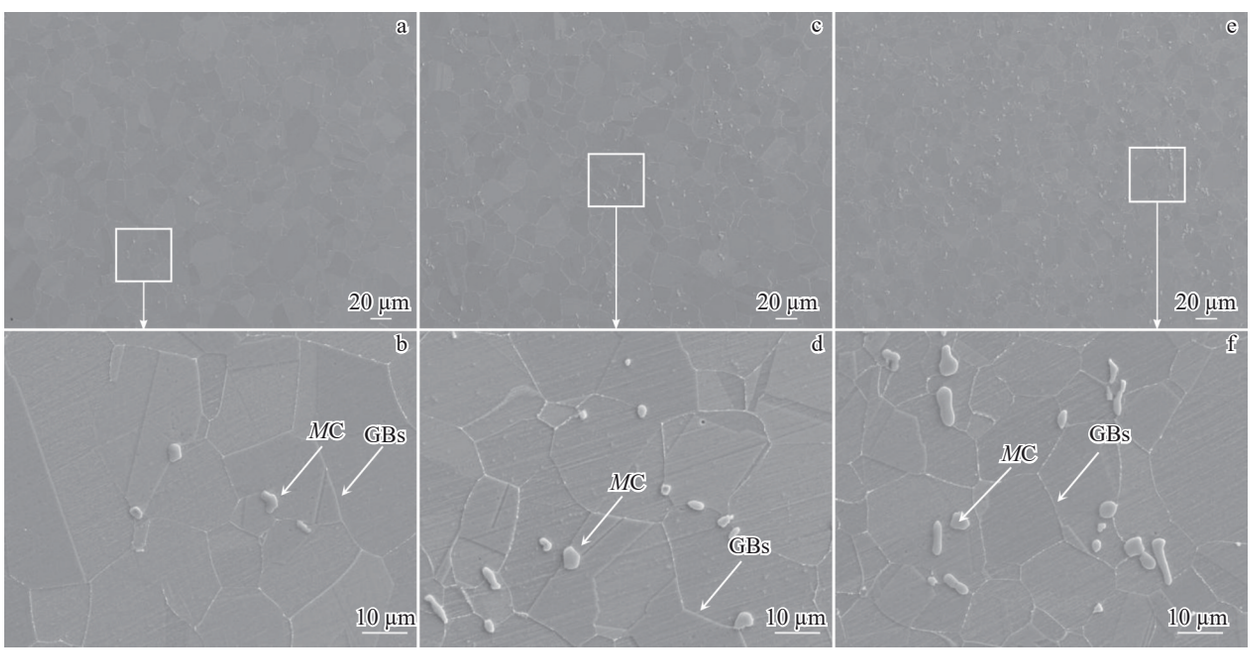

Fig.4 SEM images of precipitates in hot-rolled GH4750 alloys with varying C contents: (a–b) 0.024wt%, (c–d) 0.042wt%, and (e–f) 0.082wt%

48.25at% Nb, 0.83at% Cr, and 2.58at% Mo, confirming that the particle can be identified as an *M*C-(Ti, Nb)C. In addition, a small amount of GB carbides is observed in the alloys containing 0.024wt% C, 0.042wt% C, and 0.082wt% C (Fig.4b, 4d, and 4f). These carbides, in contrast to the blocky *M*C carbides, exhibit a fine short-rod morphology with smaller dimensions and are inferred to be $M_{23}C_6$ (*M*=Cr) based on their morphology and distribution.

Fig.6 shows EBSD IPF maps of solution-treated alloys with different C contents (IPF//RD). Compared with the hot-rolled condition, the grain sizes of the solution-treated alloys increase significantly, with average grain sizes of 184.52, 161.96, and 92.39 μm for the alloys containing 0.024wt% C, 0.042wt% C, and 0.082wt% C, respectively. The grain size of the 0.024wt% C alloy is more than twice that of the 0.082wt% C alloy, indicating that grain growth is markedly suppressed with increasing C content. According to the thermodynamic calculations in Fig. 1, the precipitation temperature of *M*C carbides is approximately 1300 °C, which is well above the solution-treatment temperature (1120 °C/4 h). Thus, *M*C carbides do not dissolve during solution treatment and continue to inhibit grain coarsening. With increasing C content, the number of *M*C carbides increases, thereby exerting a stronger pinning effect on grain growth.

Fig. 7 shows SEM microstructures of the alloys with different C contents after solution treatment and aging. With increasing C content from 0.024wt% to 0.042wt% and 0.082wt%, both the size and number of *M*C carbides increase, and their area fractions are 0.165%, 0.307%, and 0.543%, respectively. The carbides precipitated along the GBs during aging are identified as $M_{23}C_6$. As the C content increases, the morphology of $M_{23}C_6$ gradually changes from a continuous film-like distribution to a granular or chain-like distribution. To quantitatively characterize the differences in the distribution of $M_{23}C_6$ among three alloys, the $M_{23}C_6$ density (ρ) at GB, average diameter ($\bar{d}$), and average interparticle spacing ($\bar{d}_{ID}$) are calculated using the following equations:

$$\rho = \sum_1^m m_i / \left(\sum_1^m m_i + \sum_1^n n_i \right)$$

$$\bar{d} = \left(\sum_i^k d_i \right) / k$$

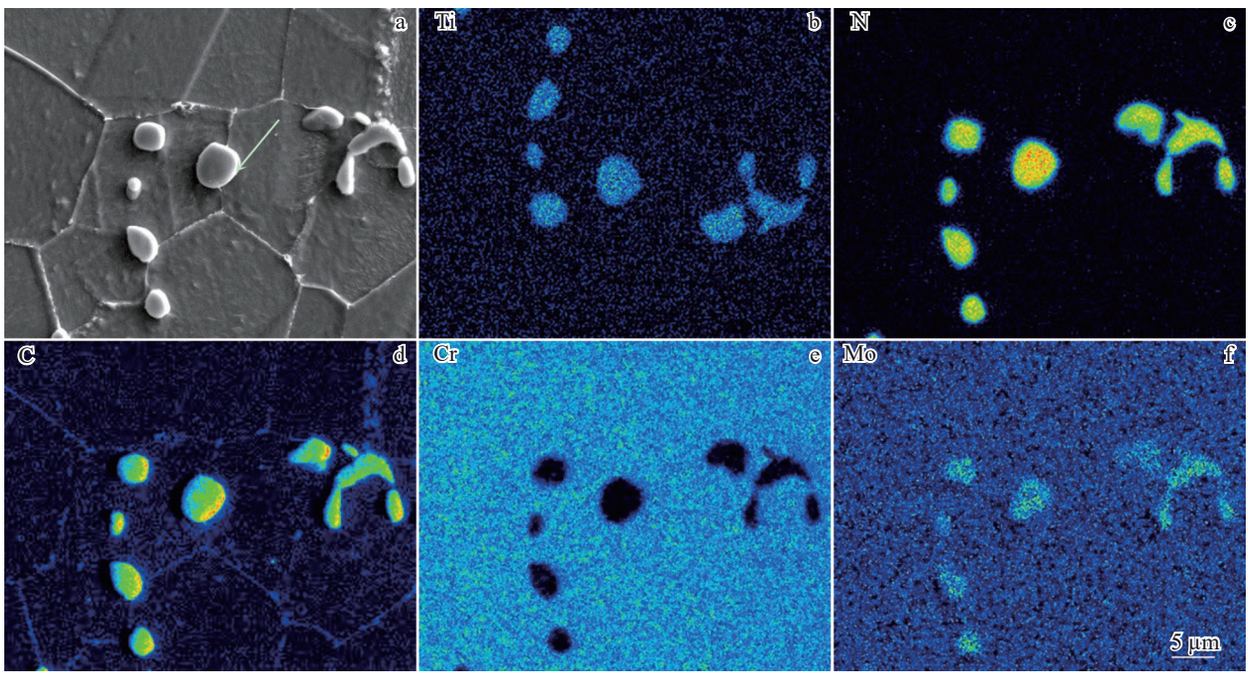

Fig.5 EPMA image (a) and corresponding EDS elemental maps (b–f) of hot-rolled GH4750 alloy containing 0.082wt% C

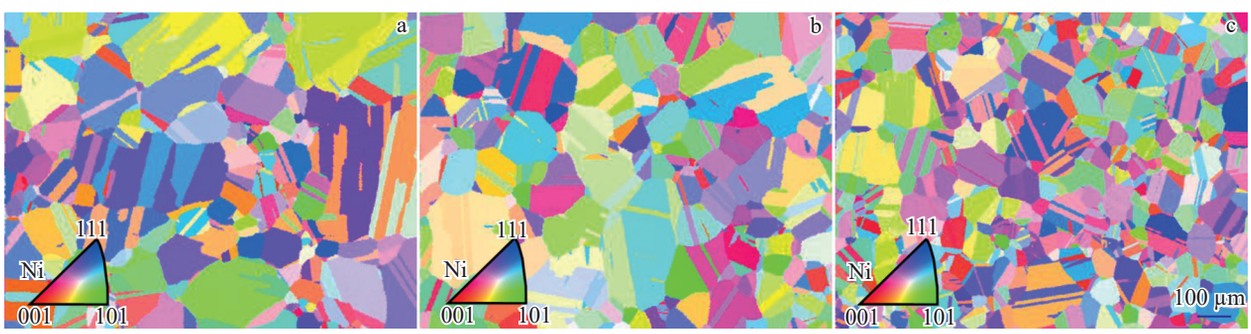

Fig.6 IPF maps showing the grain morphology of solution-treated GH4750 alloy with different C contents: (a) 0.024wt%, (b) 0.042wt%, and (c) 0.082wt%

$$d_{\mathrm{ID}} = (\sum\nolimits_i^n n_i)/n$$

where m_i represents the length of an individual $M_{23}C_6$ carbide along the GB, d_i is the diameter of $M_{23}C_6$, and n_i is the interparticle spacing of $M_{23}C_6$. With increasing C content, both ρ and $\overline{d}$ increase, while $\overline{d}_{\mathrm{ID}}$ decreases, indicating that in high-C alloys, the $M_{23}C_6$ carbides are larger in size and distributed more densely. This suggests that higher C content promotes the precipitation of $M_{23}C_6$ carbides at GB. In addition, high-magnification SEM images reveal that spherical γ' phases are uniformly dispersed within the γ matrix (Fig. 7c, 7f, and 7i). Their average diameter is approximately 45 nm, and no significant differences in morphology, size, or distribution of γ' phases are observed among alloys with different C contents.

Fig. 8 shows XRD patterns of GH4750 alloys with different C contents after solution and aging treatments. The three strong diffraction peaks located at 2θ =44°, 51°, and 75° correspond to the (111), (200), and (220) planes of the face-centered cubic (fcc) γ matrix (a=0.359 nm, JCPDS 47-1417), indicating the presence of the γ phase in the alloy. The γ' phase also exhibits an fcc structure (a=0.358 nm, JCPDS 18-0872). Because the lattice parameters of the γ matrix and γ' phase are extremely close, their three main diffraction peaks overlap. Within the XRD detection limit, no diffraction peaks corresponding to MC or $M_{23}C_6$ precipitates are observed, likely due to their relatively low volume fractions, which render them undetectable by XRD.

The elemental distribution and crystal structure of MC, $M_{23}C_6$ carbides, and γ' phase in the GH4750 alloy are characterized by TEM, as shown in Fig.9. Based on elemental mapping and selected area electron diffraction (SAED) analysis (Fig.9a, 9c, and 9e), the fine intragranular blocky MC carbides are enriched in Ti, Nb, and C, and possess a fcc structure. The fine-grained $M_{23}C_6$ carbides located at GBs are enriched mainly in Cr and also exhibit a complex fcc structure. The uniformly distributed intragranular spherical γ' phases are enriched in Al, Ni, and Ti and exhibit an $L1_2$ ordered structure. From high-resolution TEM (HRTEM) images of MC, $M_{23}C_6$ carbides, and γ' phase (Fig. 9b, 9d, and

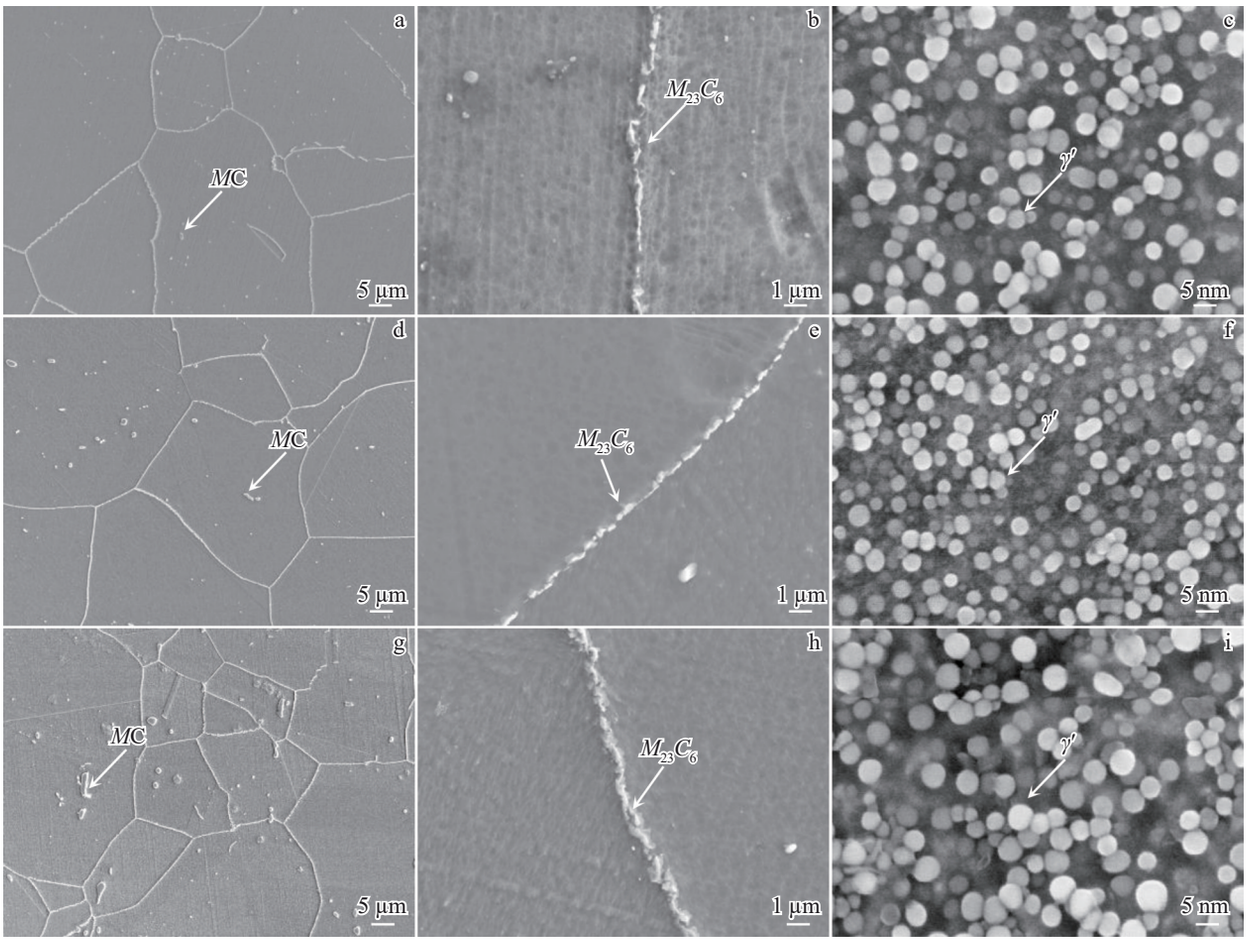

Fig.7 SEM images of precipitates in the heat-treated GH4750 alloys with varying C contents: (a – c) 0.024wt% , (d – f) 0.042wt% , and (g–i) 0.082wt%

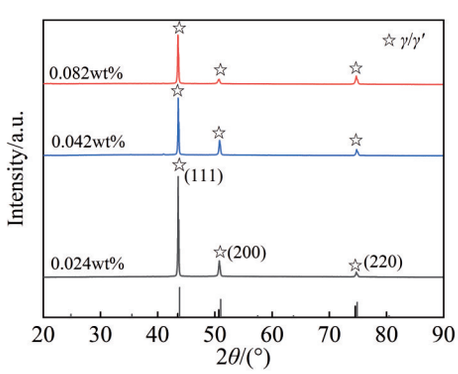

Fig.8 XRD patterns of precipitates in the heat-treated GH4750 alloys with varying C contents

9f), the interplanar spacing is determined by measuring the distance between adjacent bright fringes in locally magnified regions. For *M*C carbides, the measured $d_{(200)}$ =0.223 nm, corresponding to a lattice parameter of 0.434 nm. For $M_{23}C_6$ carbides, $d_{(111)}$ =0.566 nm, yielding a lattice parameter of 0.973 nm. For the γ' phase, $d_{(200)}$ =0.180 nm, giving a lattice parameter of 0.358 nm. Moreover, the weak superlattice diffraction spots observed in SAED pattern (Fig. 9e) indicate that nanoscale γ' phases precipitate dispersively from the supersaturated γ matrix during aging. The γ' phase is coherent with the γ matrix, with the orientation relationship of [100]γ// [100]γ' and <010>γ//<010>γ'. It is noteworthy that enrichment of Al, Ni, and Ti is observed around the $M_{23}C_6$ carbides (blue box in Fig. 9c), indicating that γ' phases surround $M_{23}C_6$ carbides. From the perspective of elemental diffusion, this phenomenon occurs because the precipitation of $M_{23}C_6$ carbides consumes Cr and Mo, leading to local enrichment of Al and Ti, which are key γ' -forming elements, in the surrounding matrix. The corresponding phase transformation can be described as $\gamma \rightarrow M_{23}C_6+\gamma'$. Although the reaction *M*C+γ $\rightarrow M_{23}C_6+\gamma'$ is also thermodynamically possible, no *M*C-type carbides are detected in this study (Fig. 9), suggesting that the formation of $M_{23}C_6$ is unlikely to originate from *M*C decomposition.

3.4 Tensile properties at room temperature and 750 °C

Fig. 10 presents the tensile properties of three C-modified alloys after the standard heat treatment at room temperature and 750 °C. The C content has only a minor effect on the yield strength (YS) and ultimate tensile strength (UTS) of GH4750 alloy, although both generally show a trend of first increasing and then decreasing. The 0.024wt% C and 0.082wt% C alloys exhibit relatively lower tensile strengths. The elongation (*A*)

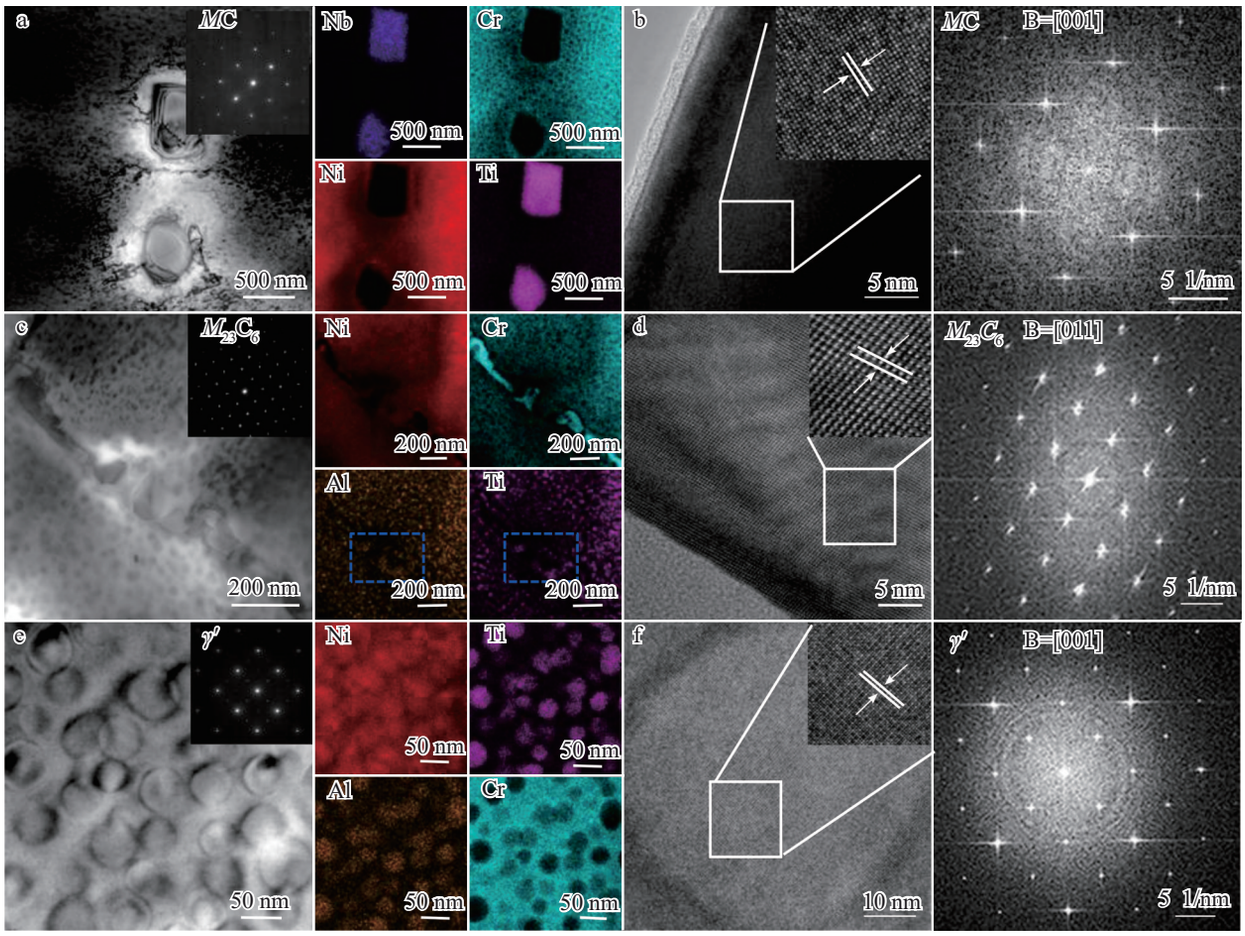

Fig.9 Characterization of precipitates in the heat-treated GH4750 alloy containing 0.042wt% C: (a–b) *M*C carbides within the grain, (c–d) $M_{23}C_6$ carbides at the GB, and (e–f) γ' phase

values at room temperature and 750 °C are relatively high, ranging from 20% to 26% and from 18% to 27%, respectively. The reduction of area (*Z*) shows only slight variation, ranging from 18% to 22% at room temperature and from 25% to 32% at 750 °C. Overall, when the C content is 0.042wt%, the GH4750 alloy exhibits superior tensile strength at both room temperature and 750 °C while maintaining good tensile ductility.

The variation in alloy strength results from the accumulation and motion of dislocations. The underlying mechanism of the grain size effect is that moving dislocations within grains are blocked at GBs, where they pile up. Once a sufficient number of dislocations accumulate, the resulting stress activates dislocation sources in neighboring grains. This cyclic process of dislocation motion gradually accumulates, ultimately leading to plastic deformation. A reduction in grain size increases the number of GBs, thereby introducing more obstacles to dislocation motion. Consequently, a higher stress is required to initiate plastic deformation, which macroscopically manifests as enhanced alloy strength. In other words, smaller grain size corresponds to higher YS, as described by the Hall-Petch relationship. In the GH4750 alloy, the grain size decreases with increasing C content. The GB strengthening effect in the alloy containing 0.082wt% C is greater than that in the lower-C alloys. Therefore, it might be expected that the alloy containing 0.082wt% C will exhibit higher YS compared with the other alloys. However, in practice, YS of the 0.082wt% C alloy is lower than that of the 0.024wt% C and 0.042wt% C alloys. This phenomenon indicates that multiple factors, beyond grain size, influence the alloy's tensile strength. Among these, the role of second-phase particles, particularly *M*C carbides, is of critical importance and often competes with grain refinement in determining the overall mechanical response.

The strengthening mechanism of the second phase is generally similar to that of grain-size refinement, with its effectiveness depending on factors such as particle number, size, morphology, and crystallographic relationships with the matrix. To clarify the primary crack initiation sites during fracture, EBSD was performed on longitudinal sections slightly away from the fracture region. The kernel average misorientation (KAM) maps, which reflect dislocation density, are used to evaluate the level of stress concentration[30]. In these maps, blue regions represent lower dislocation densities, whereas green and red regions indicate higher dislocation densities. The significant atomic misfit at GBs makes them

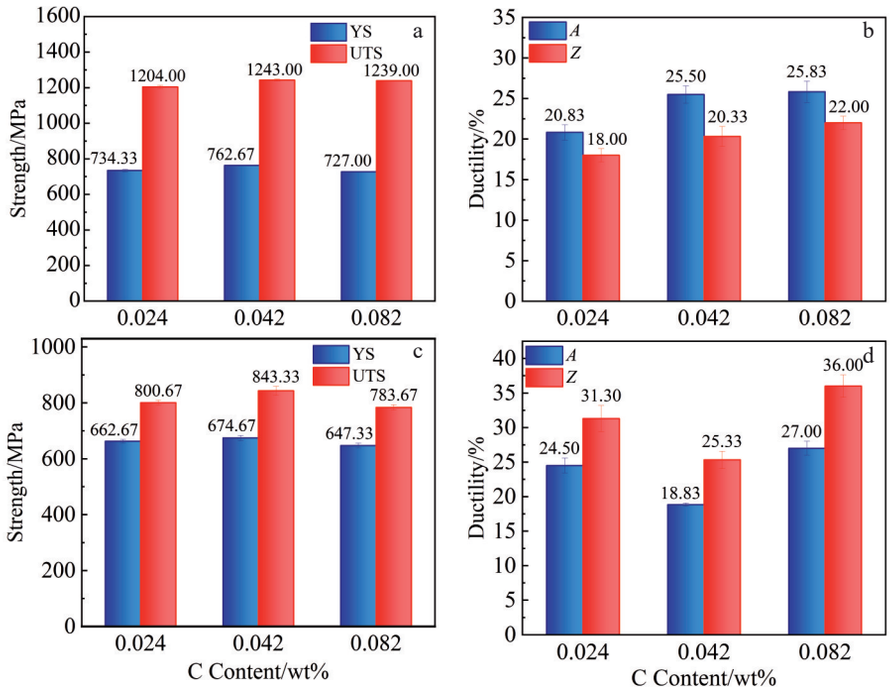

Fig.10 Comparison chart of tensile properties of GH4750 alloys with varying C contents after standard heat treatment at room temperature (a–b) and 750 °C (c–d): (a, c) YS and UTS; (b, d) elongation (*A*) and reduction of area (*Z*)

preferential sites for strain accumulation during plastic deformation[31]. Once the local dislocation density reaches saturation, void formation becomes almost inevitable in the 0.024wt% C alloy, and intergranular fracture features are observed, which are associated with continuous dislocation accumulation at GBs. GB cracking occurs through the nucleation, growth, and coalescence of microvoids (Fig. 11a–11d). Due to the large lattice mismatch between *M*C carbides and the γ matrix, stress concentration develops at the interface[32]. During plastic deformation, dislocations accumulate around *M*C carbides, further intensifying interfacial stress concentration. This eventually leads to decohesion at the *M*C/γ matrix interface and the formation of voids. As these voids expand and coalesce, larger cavities develop, and once a critical size is reached or linkage occurs, fracture is initiated.

In contrast, in the 0.042wt% C alloy, *M*C carbides along the GBs exhibit moderate size and spacing. No significant interfacial microcracks are detected between *M*C carbides and the matrix, with only a small number of microvoids observed. This effectively alleviates stress concentration caused by dislocation pile-up and separates voids, thereby impeding their growth into microcracks (Fig. 11e–11h). The combined effects of grain refinement strengthening and second phase strengthening result in the superior strength of the 0.042wt% C alloy compared with the 0.024wt% C alloy. In the 0.082wt% C alloy, however, massive dislocation pile-up at *M*C/γ interfaces promotes the formation of voids. Some dislocations can shear into *M*C carbides, which accelerates the nucleation of internal microcracks originating from voids. Under applied stress, these internal microcracks propagate, leading to the fracture of the *M*C carbide and leaving cavities behind. This significantly weakens the interfacial bonding between *M*C carbides and the γ matrix, thereby severely degrading the alloy's properties (Fig. 11i–11l). Although grain refinement improves strength, the data clearly show that the detrimental effect of *M*C carbides outweighs the beneficial effect of grain-size reduction. Overall, the tensile behavior of GH4750 alloys with different C contents is governed by the interplay between grain size and *M*C carbide characteristics: intergranular fracture dominates in the low-C alloy, and optimized carbide distribution enhances strength in the medium-C alloy. At the same time, excessive carbide-induced damage deteriorates the mechanical performance in the high-C alloy.

It is well known that at elevated temperatures, GBs are weaker than the grain interiors, making them the weak link during deformation. Due to thermal diffusion, the atomic arrangement in the GB region is disrupted, leading to vacancies, solute segregation, and other microdefects. Moving dislocations pile up at the GB, but quickly interact with these defects and vanish, meaning that the resistance of GBs to dislocation motion decreases with increasing temperature. As a result, GBs tend to slide and migrate, giving rise to pronounced boundary deformation. The precipitation of $M_{23}C_6$ carbides along GBs restricts GB sliding and migration, while simultaneously healing microdefects and reducing the adverse effects of solute segregation. Segregated impurity elements at GBs are either divided by the carbides or incorporated into them. The $M_{23}C_6$/γ interfaces also serve as favorable sites for dislocation pile-up; only after a sufficient number of dislocations accumulate and stress concentration reaches a critical level, does GB sliding occur, enabling grain deformation and resulting in observable macroscopic strain.

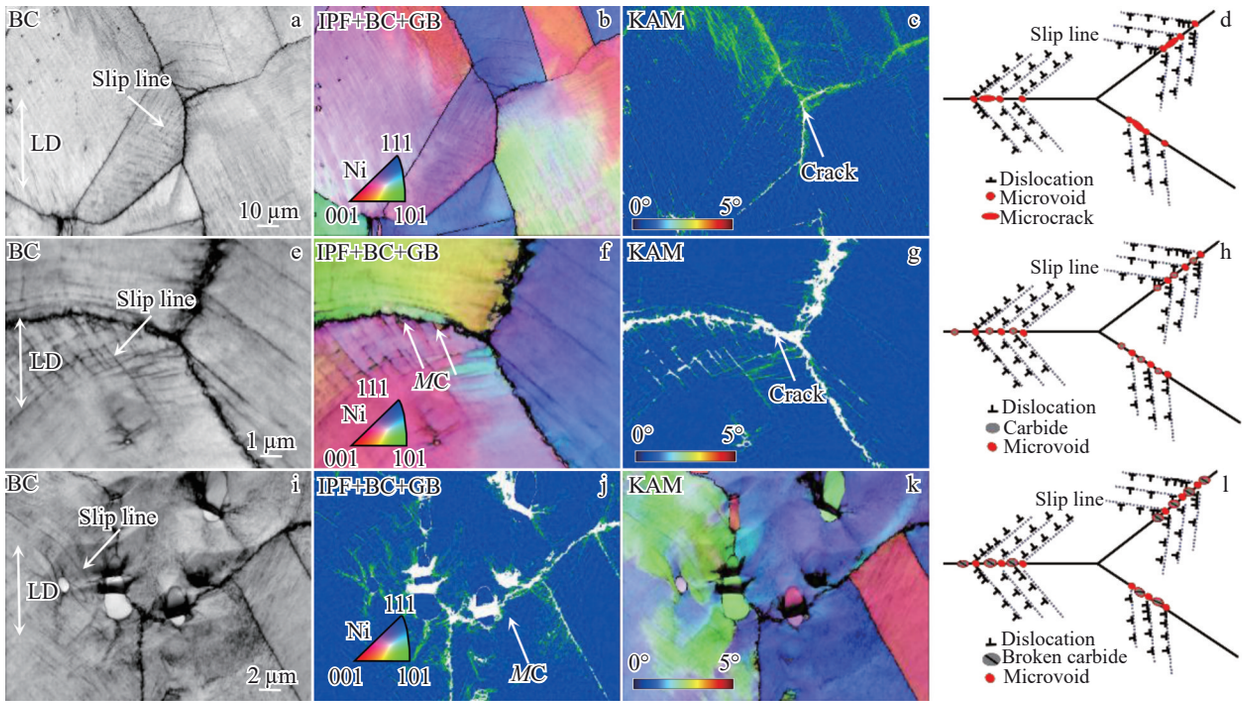

Fig.11 EBSD analysis results of longitudinal microstructure in GH4750 alloy samples after room-temperature tensile testing and corresponding fracture schematics: (a–d) 0.024wt% C, (e–h) 0.042wt% C, and (i–l) 0.082wt% C (BC refers to band contrast; LD refers to loading direction)

More importantly, $M_{23}C_6$ carbides delay microvoid coalescence and reduce crack propagation rates. During tensile deformation, microvoids form in the GB region, readily grow, link, and propagate into microcracks. However, crack growth is hindered at $M_{23}C_6/\gamma$ interfaces, slowing the overall propagation rate. In alloys with low C content, the density of $M_{23}C_6$ carbides at GBs is low, and the interparticle spacing is large, thereby weakening their ability to resist microcrack growth and coalescence. Once cracks extend beyond a critical threshold, fracture occurs, leading to poor high-temperature strength in such alloys.

Furthermore, in low-C alloys, elongated carbides form film-like structures that tend to rupture under external stress, thereby serving as preferential sites for crack initiation. With increasing C content, carbides predominantly exhibit a granular morphology with reduced spacing, thereby significantly impeding crack propagation and enhancing high-temperature strength. However, in alloys with 0.082wt% C, chain-like $M_{23}C_6$ carbides form at GBs, facilitating intergranular cracking and thereby degrading the alloy's mechanical performance.

Fig. 12 presents EBSD maps of fractured tensile samples (750 ° C) for alloys with 0.024wt% C, 0.042wt% C, and 0.082wt% C. All three alloys exhibit intergranular cracks, consistent with slip activation in high-Schmid factor (SF) grains and limited plasticity in low-SF grains. At elevated temperature, GB sliding further promotes crack formation. As reported previously[33], voids generated by sliding preferentially nucleate along favorable boundary orientations rather than strictly parallel to the stress axis, which explains the inclined cracks observed (Fig. 12a, 12f, and 12k) in the 0.024wt% C alloy; insufficient carbide pinning allows pronounced boundary sliding, facilitating crack initiation and rapid failure, and increasing C content to 0.042wt% enhances *M*C carbide precipitation, which strengthens boundaries and delays void nucleation. In contrast, the 0.082wt% C alloy contains a high volume fraction of carbides, but their continuous morphology impedes stress transfer, concentrating stress at *MC*/γ interfaces and accelerating void formation. The refined grain size further increases the boundary area, providing additional crack-propagation paths and promoting intergranular fracture.

3.5 High-temperature creep behavior

Fig. 13 shows the creep performance of the three C-modified alloys after standard heat treatment under a complex stress condition at 750 ° C/320 MPa. Creep life decreases with increasing C content: the 0.024wt% C alloy exhibits the longest life (964 h), the 0.042wt% C alloy shows a comparable life (864 h), while the 0.082wt% C alloy has the shortest life (631 h). All alloys display the typical three creep stages: primary decelerating creep, secondary steady-state creep, and tertiary accelerating creep. The 0.024wt% C alloy exhibits the longest steady-state stage and the lowest steady-state creep rate. Considering both tensile and creep performance, a C content of 0.042wt% is identified as the optimal composition.

Fig.14 presents EBSD analysis results for the microstructure parallel to the stress axis in creep-ruptured alloys containing

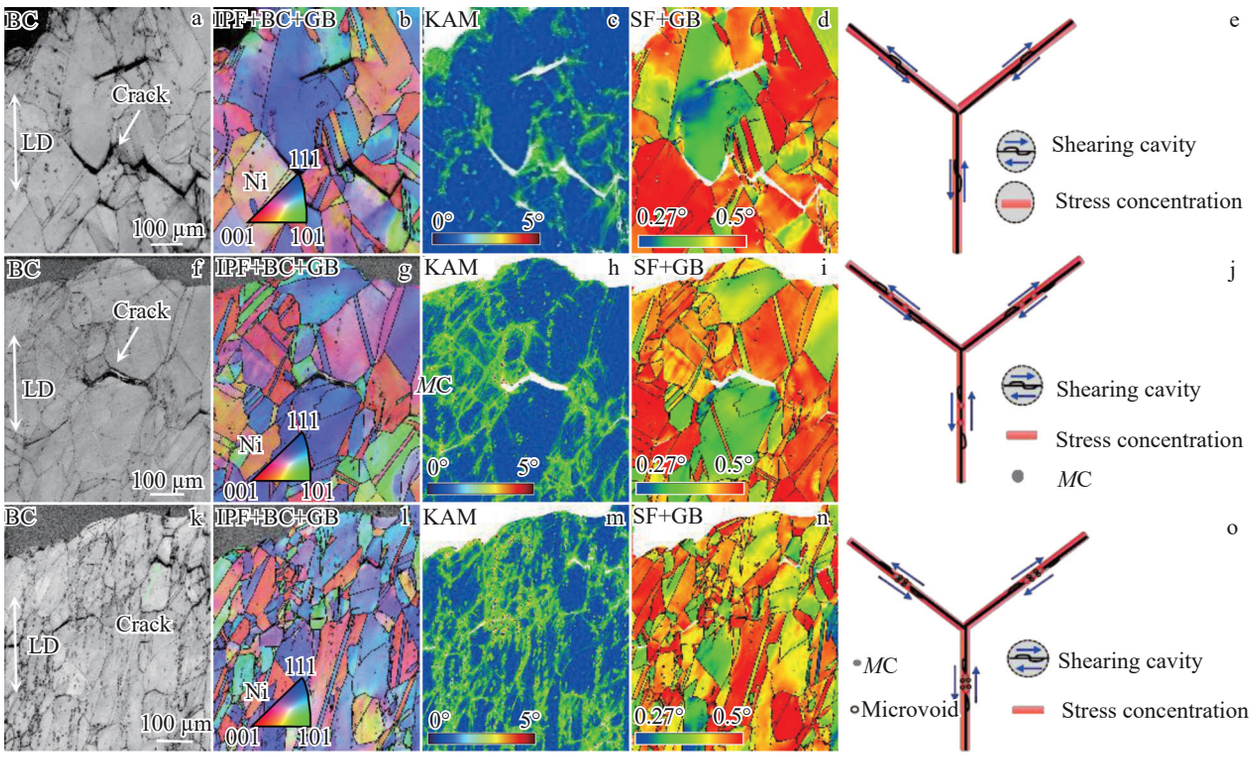

Fig.12 EBSD analysis results of longitudinal microstructure in GH4750 alloy samples after tensile testing at 750 ℃ and corresponding fracture schematics: (a–e) 0.024wt% C, (f–j) 0.042wt% C, and (k–o) 0.082wt% C (SF refers to stacking fault)

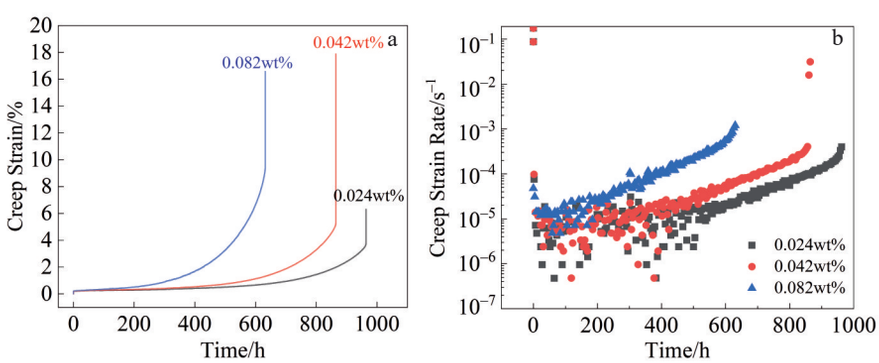

Fig.13 Creep strain (a) and creep strain rate (b) versus time for GH4750 alloys with various C contents under 750 ℃ and 320 MPa

0.024wt% C, 0.042wt% C, and 0.082wt% C tested at 750 °C and 320 MPa. As the C content increases from 0.024wt% to 0.082wt% , the average grain size of the heat-treated alloy decreases significantly. The reduction in grain size increases the number of GBs per unit volume, which in turn leads to a higher quantity of GB carbides. The presence of coarse *M*C carbides induces stress concentration at the *M*C/*γ* interfaces, promoting the formation of microvoids. This results in more potential sites for microvoid and microcrack nucleation along GBs, which is detrimental to stress-rupture life.

The formation of voids or cracks at *M*C carbides is primarily attributed to their larger lattice constant relative to the matrix, which weakens interfacial bonding and facilitates decohesion. Excessive precipitation of *M*C carbides increases their distribution along GBs, thereby raising the probability of void or crack formation and promoting secondary cracking. Moreover, studies[25,34–35] have reported that precipitation of GB carbides depletes solid-solution strengthening elements from the *γ* matrix, thereby reducing the interfacial cohesion between the matrix and carbides. Hence, *M*C carbides at GB serve as potential nucleation sites for microvoids and microcracks under stress accumulation.

Statistical results of the distribution and area fraction of *M*C carbides indicate that the area fraction of *M*C carbides increases with increasing C content. During creep deformation, dislocations accumulate around *M*C carbides, weakening the interfacial bonding and facilitating void initiation. This accelerates void coalescence and crack formation. A greater number and larger size of *M*C carbides increase the number of potential void nucleation sites, thereby raising the likelihood of crack formation. This explains the relatively shorter stress-rupture life of the GH4750 alloy

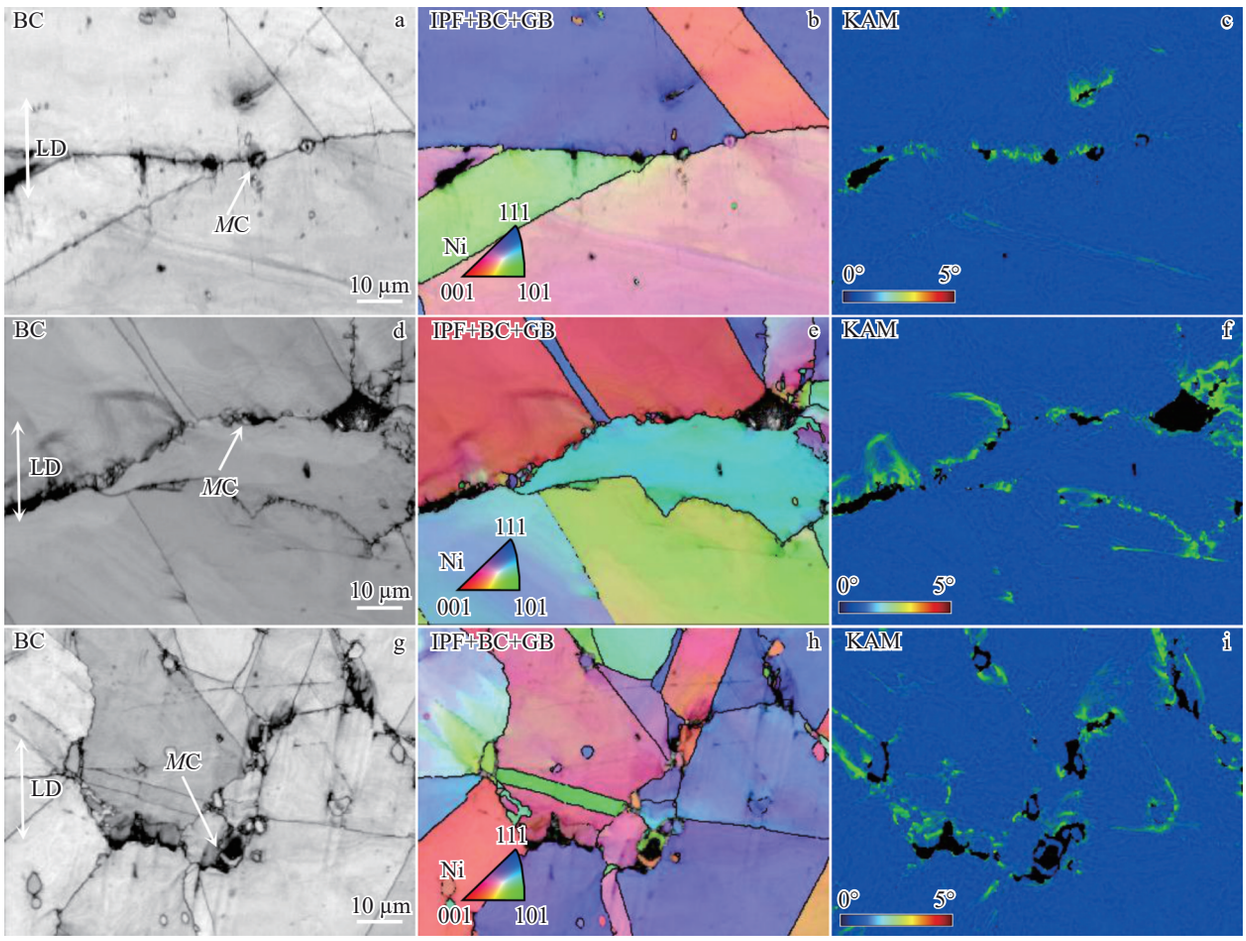

Fig.14 EBSD analysis results of longitudinal microstructure in GH4750 alloy samples after stress rupture test at 750 °C under the stress of 320 MPa: (a–c) 0.024wt% C; (d–f) 0.042wt% C, and (g–i) 0.082wt% C

containing 0.082wt% C. More importantly, studies[27–28] have reported that larger grain sizes improve creep resistance and lead to longer stress-rupture lives. As the grain size of the Ni-Cr-W-Fe alloy decreases with increasing C content, the rupture life of high-C alloys is adversely affected by finer grain sizes.

4 Conclusions

1) As the C content increases from 0.024wt% to 0.082wt%, the types of phases in the GH4750 alloy remain unchanged. The liquidus temperature decreases from 1364 °C to 1361 °C, the precipitation temperature of *M*C carbides increases from 1270 °C to 1310 °C, and the precipitation temperature of the γ' phase decreases from 1000 °C to 993 °C.

2) With the increase in C content from 0.024wt% to 0.082wt%, the area fraction of *M*C carbides in the hot-rolled alloy increases from 0.197% to 0.701%, and their morphology transitions from small blocky to large blocky or rod-like shapes. The increased *M*C carbides enhance their pinning effect on GB migration, thereby reducing the average grain size of the hot-rolled alloy from 35.11 μm to 22.05 μm. Furthermore, higher C content promotes the precipitation of $M_{23}C_6$ carbides during the heat treatment of GH4750 alloy, changing their morphology from a continuous film to discrete particles along the GBs.

3) The tensile strength at room temperature and 750 °C initially increases and then decreases with increasing C content, while the elongation exhibits the opposite trend. During room-temperature tensile tests, strength is influenced by both grain refinement and second-phase strengthening; however, in the 0.082wt% C alloy, the detrimental effect of *M*C carbides outweighs the beneficial effect of grain refinement. During high-temperature (750 °C) tensile tests, GB sliding becomes the dominant fracture mechanism. Although increased carbide content can hinder GB sliding, excessive continuous carbides can cause stress concentration and decohesion, leading to microcrack formation and a degradation of mechanical properties.

4) The creep life decreases with increasing C content. Finer grain sizes increase the number of GBs per unit volume, which in turn raises the quantity of GB carbides. The presence of coarse *M*C carbides induces stress concentration at the *MC*/γ interfaces, promoting microvoid formation. Consequently, more potential sites for microvoid and microcrack nucleation are present along GBs, which is detrimental to stress-rupture life.

References

1 Pollock T M, Tin S. *Journal of Propulsion and Power*[J], 2006, 22(2): 361
2 Reed R C. *The Superalloys: Fundamentals and Applications*[M]. Cambridge: Cambridge University Press, 2008
3 Zhao J C, Westbrook J H. *MRS Bulletin*[J], 2003, 28(9): 622
4 An Junjing, Chen Jiacheng, Wang Huisheng *et al. Nuclear Science and Engineering*[J], 2025, 45(3): 527 (in Chinese)
5 Xiao W K, Wu Shidong. *Foreign Ship Technology* (*Materials*)[J], 1980(4): 42 (in Chinese)
6 Amiri A, Bruschi S, Sadeghi M H *et al. Materials Science and Engineering A*[J], 2013, 562: 77
7 Yang J, Zheng Q, Ji M *et al. Materials Science and Engineering A*[J], 2011, 528(3): 1534
8 Tian B, Lind C, Paris O. *Materials Science and Engineering A*[J], 2003, 358(1–2): 44
9 Lvov G, Levit V, Kaufman M. *Metallurgical and Materials Transactions A*[J], 2004, 35(6): 1669
10 Wei C N, Bor H Y, Chang L. *Journal of Alloys and Compounds*[J], 2011, 509(18): 5708
11 Ou M, Ma Y, Ge H *et al. Journal of Alloys and Compounds*[J], 2018, 735: 193
12 Zhong Z, Gu Y, Yuan Y *et al. Metallurgical and Materials Transactions A*[J], 2014, 45(1): 343
13 Kim D M, Kim C, Yang C H *et al. Journal of Alloys and Compounds*[J], 2023, 946: 169341
14 Wang W, Hong H, Kim I *et al. Materials Science and Engineering A*[J], 2009, 523(1–2): 242
15 Unocic K, Kirka M, Cakmak E *et al. Materials Science and Engineering A*[J], 2020, 772: 138607
16 Zhang P, Yuan Y, Gu Y F *et al. Journal of Alloys and Compounds*[J], 2020, 825: 154012
17 Tin S, Pollock T, Murphy W. *Metallurgical and Materials Transactions A*[J], 2001, 32: 1743
18 Shulga A. *Journal of Alloys and Compounds*[J], 2007, 436(1–2): 155
19 Al-Jarba K, Fuchs G. *Materials Science and Engineering A*[J], 2004, 373(1–2): 255
20 Zhao G, Zang X, Jing Y *et al. Materials Science and Engineering A*[J], 2021, 815: 141293
21 Dong X, Zhang X, Du K *et al. Journal of Materials Science & Technology*[J], 2012, 28(11): 1031
22 Qin X Z, Guo J T, Yuan C *et al. Metallurgical and Materials Transactions A*[J], 2007, 38: 3014
23 Liu L R, Jin T, Zhao N R *et al. Materials Science and Engineering A*[J], 2003, 361(1–2): 191
24 Guo Jianting, Zhang Jinyan, Huang Rongfang *et al. Acta Metallurgica Sinica*[J], 1985(6): 1 (in Chinese)
25 Yang J, Zheng Q, Sun X *et al. Materials Science and Engineering A*[J], 2006, 429(1–2): 341
26 Lim Y S, Kim D J, Hwang S S *et al. Materials Characterization*[J], 2014, 96: 28
27 Gibbons T, Hopkins B. *Metal Science*[J], 1984, 18(5): 273
28 Shingledecker J, Evans N, Pharr G. *Materials Science and Engineering A*[J], 2013, 578: 277
29 Qin X Z, Guo J T, Yuan C *et al. Materials Science and Engineering A*[J], 2008, 485(1–2): 74
30 Chen X, Yao Z, Dong J *et al. Journal of Alloys and Compounds*[J], 2018, 735: 928
31 Rakhmonov J U, Bahl S, Shyam A *et al. Acta Materialia*[J], 2022, 228: 117788
32 Wang Liang, Hu Yiwen, Zhou Peishan *et al. Rare Metal Materials and Engineering*[J], 2025, 54(4): 1015 (in Chinese)
33 Wang L, Hu Y W, Zhou P S *et al. Metallurgical and Materials Transactions A*[J], 1999, 30(3): 829
34 D'Souza N, Kantor B, West G *et al. Journal of Alloys and Compounds*[J], 2017, 702: 6
35 Ling Chen, Li Shangping, Lin Jun *et al. Rare Metal Materials and Engineering*[J], 2024, 53(3): 815 (in Chinese)

碳含量对一种变形镍基高温合金组织性能的影响

刘文丽[1,2,3]，赵　霞[2,3]，侯坤磊[2,3]，王一飞[4]，王　平[1]，马颖澈[2,3]，郝宪朝[2,3]，欧美琼[2,3]

（1. 东北大学 材料科学与工程学院，辽宁 沈阳 110819）

（2. 中国科学院 金属研究所 师昌绪先进材料创新中心，辽宁 沈阳 110016）

（3. 中国科学院 金属研究所 核用材料与安全评价重点实验室，辽宁 沈阳 110016）

（4. 中机试验装备股份有限公司，吉林 长春 130103）

摘　要：碳（C）作为镍基高温合金中重要的微量元素，其含量的微小变化对合金力学性能具有显著影响。考察了C含量对新型镍基高温合金GH4750显微组织与力学性能的作用规律。结果表明：随着C含量从0.024wt%提升至0.042wt%进而增至0.082wt%，碳化物的含量和平均尺寸增加，并且碳化物钉扎晶界，使晶粒尺寸从约35 μm降低到约31 μm，再降低到约22 μm。室温和750 ℃的抗拉伸强度随C含量增加呈现先升高后降低的趋势，而延伸率则表现出相反的变化规律。抗拉伸性能的差异与碳化物的特征密切相关：适量增加碳化物一方面能抑制微孔洞的形成与连接，另一方面能钉扎晶界，阻碍高温下晶界的滑移变形，但过量的碳化物则可能成为裂纹源，恶化性能。750 ℃/320 MPa蠕变寿命随C含量的增加单调降低，这归因于较大的晶粒尺寸更有利于提升合金的抗蠕变性能。综合考量，确定该新型镍基高温合金GH4750的最佳碳含量为0.042wt%。

关键词：镍基高温合金；碳含量；力学性能；断裂机理

作者简介：刘文丽，女，2000年生，硕士，东北大学材料科学与工程学院，辽宁 沈阳 110819，E-mail：15041384435@163.com